JOURNAL OF Materials CHEMISTRY

Structural approach of the features of the spin crossover transition in iron(II) compounds

Philippe Guionneau,[a,b] Jean-François Létard,[b] Dimitrii S. Yufit,[a] Daniel Chasseau,[b] Georges Bravic,[b] Andrés E. Goeta,[a] Judith A. K. Howard[a] and Olivier Kahn[b]

[a]*Chemical Crystallography Group, Chemistry Department, Durham University, South Road, Durham, UK DH1 3LE*
[b]*Laboratoire des Sciences Moléculaires, Institut de Chimie de la Matière Condensée de Bordeaux, UPR CNRS 9048, 33608 Pessac, France*

Received 19th October 1998, Accepted 27th January 1999

We have determined the crystal structures, both in high and low spin state, of four $Fe(PM\text{-}L)_2(NCS)_2$ complexes, where PM is *N*-2′-pyridylmethylene and the aromatic subunit L is 4-aminoterphenyl (TeA), 4-(phenylazo)aniline (AzA), 4-aminobiphenyl (BiA) or 4-(phenylethynyl)aniline (PEA). As previously reported, these compounds undergo a spin crossover at low temperature with different features of transition: very smooth and incomplete for $Fe(PM\text{-}TeA)_2(NCS)_2$, smooth with almost no hysteresis for $Fe(PM\text{-}AzA)_2(NCS)_2$, unusually abrupt for $Fe(PM\text{-}BiA)_2(NCS)_2$ and abrupt with a very large hysteresis (37 K) for $Fe(PM\text{-}PEA)_2(NCS)_2$. In $Fe(PM\text{-}BiA)_2(NCS)_2$, $Fe(PM\text{-}TeA)_2(NCS)_2$ and $Fe(PM\text{-}AzA)_2(NCS)_2$ the spin conversion is not associated with a large structural phase transition and the space group is the same above and below the temperature of transition: orthorhombic *Pccn* for the two first and monoclinic $P2_1/c$ for the third. On the other hand, $Fe(PM\text{-}PEA)_2(NCS)_2$ undergoes a change in the crystal symmetry from $P2_1/c$ (high spin) to *Pccn* (low spin) which corresponds to a strong re-organisation of the iron atom network. The evolution as a function of temperature of the FeN_6 core as well as of the intramolecular characteristics are almost identical in all four compounds. To a first approximation, the crystal packing is similar in all of the structures except that the $P2_1/c$ structures develop an asymmetrical molecular environment. Nevertheless, a close examination of the intermolecular interactions, classified as intra- and inter-sheet, show some differences. The intrasheet and the intersheet interactions are stronger in $Fe(PM\text{-}BiA)_2(NCS)_2$ and $Fe(PM\text{-}PEA)_2(NCS)_2$ than either in $Fe(PM\text{-}TeA)_2(NCS)_2$ where no 'second' neighbour intrasheet contacts are created, or in $Fe(PM\text{-}AzA)_2(NCS)_2$ where the intersheet interactions are weak. Thus, the abruptness of the transition is attributed to the combination of close intrasheet and intersheet contacts. The hysteresis effect in $Fe(PM\text{-}PEA)_2(NCS)_2$ is connected to the phase transition which could occur due to an irregular iron atom network associated with very short carbon–carbon intermolecular contacts at high temperature, not found in $Fe(PM\text{-}AzA)_2(NCS)_2$ which shows the same irregular iron atom network.

1 Introduction

The electronic transition termed 'spin crossover' is commonly encountered among metal complexes. This phenomenon derives from the existence of two different configurations for the metallic ion characterized by different spin states. This kind of transition has been studied widely,[1] mainly for iron, cobalt, nickel and manganese complexes. For example, in d^6 metal complexes of Fe(II), it corresponds to the change in the population of the 3d orbitals from the high spin state $t^4_{2g}e^2_g$ (HS) to the low spin state $t^6_{2g}e^0_g$ (LS). In general, such a transition can be induced by thermal changes, pressure effects or exposure to electromagnetic rays and be smooth or abrupt, and possibly accompanied by hysteresis.[1] Indeed, the critical temperature of the LS to HS conversion, when warming, $T_c(\uparrow)$, could be higher than the critical temperature of the conversion from HS to LS, when cooling, $T_c(\downarrow)$; such a shift width can be of a few degrees. The diversity of features of this kind of transition offers a large range of potential applications, in optical or storage devices for example, provided that one is able to monitor the required characteristics.[2]

Some iron(II) compounds, based on triazole subunit, have been found to display thermal hysteresis widths reaching *ca.* 40 K and centered at room temperature.[3] Recently, we have designed strongly cooperative spin-crossover assemblies consisting of mononuclear molecules, with through-space rather than through-bond interactions.[4,5] In the present study, we report the X-ray structures obtained both in HS and LS state for four compounds of this type. These compounds belong to the same family of iron(II) complexes; the molecules only differ from each other in one part of the ligands (Scheme 1).

Despite the chemical similarities between the four compounds, the magnetic properties are totally different and allow us to study the topology of the intermolecular interactions on the whole range of spin crossover behaviour, starting from incomplete spin conversion to discontinuous type transitions with both narrow and wide hystereses (Fig. 1). The magnetic behaviours of the $Fe(PM\text{-}L)_2(NCS)_2$ complexes are as follows: (i) $Fe(PM\text{-}TeA)_2(NCS)_2$ **1**, *cis*-bis(thiocyanato)bis[(*N*-2′-pyridylmethylene)-4-(aminoterphenyl)]iron(II), $FeC_{50}H_{36}N_6S_2$, presents a very smooth and incomplete spin conversion; (ii) $Fe(PM\text{-}AzA)_2(NCS)_2$ **2**, *cis*-bis(thiocyanato)bis[(*N*-2′-pyridylmethylene)-4-(phenylazo)aniline]iron(II), $FeC_{38}H_{28}N_{10}S_2$, shows a very gradual complete spin conversion, with a weak hysteresis of 6 K: $T_c(\downarrow) = 186$ K and $T_c(\uparrow) = 192$ K;[6] (iii) $Fe(PM\text{-}BiA)_2(NCS)_2$ **3**, *cis*-bis(thiocyanato)bis[(*N*-2′-pyridylmethylene)-4-(aminobiphenyl)]iron(II), $FeC_{38}H_{28}N_6S_2$, undergoes an unsually abrupt transition with a very sharp hysteresis: $T_c(\downarrow) = 168$ K, $T_c(\uparrow) = 173$ K;[5] (iv) $Fe(PM\text{-}PEA)_2(NCS)_2$ **4**, *cis*-bis(thiocyanato)bis[(*N*-2′-pyridylmethylene)-4-(phenylethynyl)aniline]iron(II), $FeC_{42}H_{28}N_6S_2$, presents a very large hysteresis as well as a relatively high transition temperature: $T_c(\downarrow) = 194$ K, $T_c(\uparrow) = 231$ K.[4]

This series of iron(II) compounds provides an ideal chance to perform a complete crystallographic study on very similar compounds with different magnetic behaviours. The crystal structures of **3** at 298 and 140 K have been reported

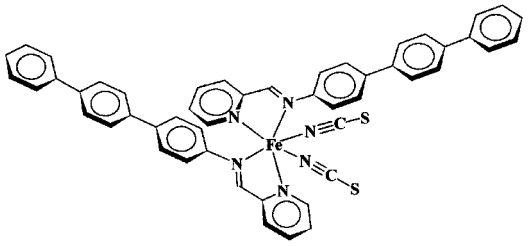

$Fe(PM\text{-}TeA)_2(NCS)_2$ **1**

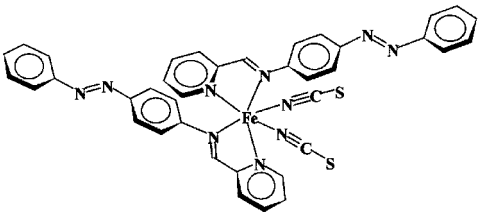

$Fe(PM\text{-}AzA)_2(NCS)_2$ **2**

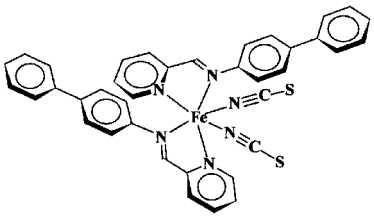

$Fe(PM\text{-}BiA)_2(NCS)_2$ **3**

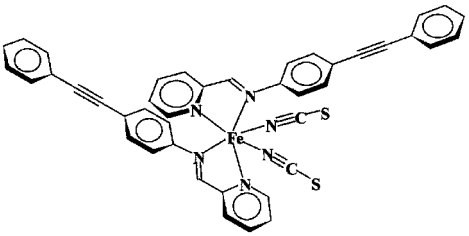

$Fe(PM\text{-}PEA)_2(NCS)_2$ **4**

Scheme 1 Schematic representation of the four $Fe(PM\text{-}L)_2(NCS)_2$ compounds **1–4**.

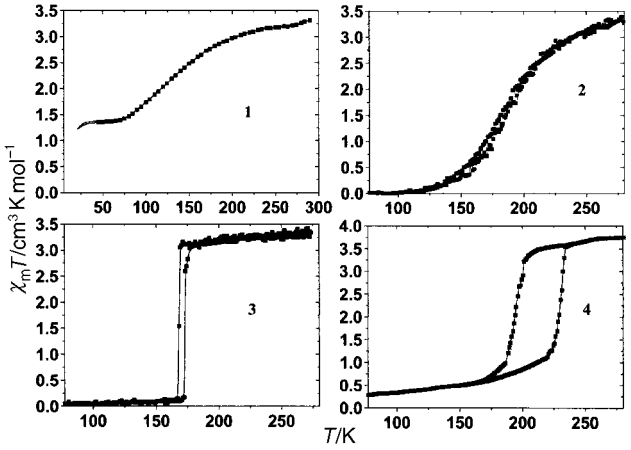

Fig. 1 $\chi_M T$ *vs.* T plot for the four studied compounds (χ_M = molar magnetic susceptibility, T = temperature).

previously.[5,7] The space group, *Pccn*, is the same at all temperatures. The spin transition corresponds to an increase of the *c* parameter leading to a change in the iron atom network. The crystal structures in the two spin states appear quite compact as a result of short C–C contacts in the intrasheet and the intersheet directions with the main change upon cooling affecting the iron atom intramolecular environment.

In the present article, we report the crystal structures of $Fe(PM\text{-}PEA)_2(NCS)_2$ **4**, $Fe(PM\text{-}AzA)_2(NCS)_2$ **2** and $Fe(PM\text{-}TeA)_2(NCS)_2$ **1** in the high spin state (at 298 K) and in the low spin state (at 140, 110 and 11 K, respectively). We also report on the thermal dilatation of the cell of **4** from 298 to 110 K as well as on some powder diffraction measurements on this compound. Additionally, we have solved the structure of **1** at 140 K in order to compare it with the low temperature structures of the three other compounds solved in this temperature range. The aim of the discussion is then to compare the structural behaviour as a function of temperature for these four compounds.

2 Experimental

All the $Fe(PM\text{-}L)_2(NCS)_2$ compounds were prepared using a stoichiometric amount of ligand in order to avoid the possible problems encountered for $Fe(PM\text{-}BiA)_2(NCS)_2$, where two phases were obtained.[5,7]

The crystallographic study in the HS state of **1** was performed using a Siemens SMART-CCD diffractometer[8] with Mo-Kα radiation. The crystals are regular black needles and reveal a weak diffraction pattern. Two full sets of data were collected at two different temperatures: 298 and 140 K. An Oxford Cryosystem N_2 open flow cryostat was used. The lowest temperature was achieved after cooling at a rate of 2 K min^{-1}. A half sphere was collected based on ω-scans at values of $\phi = 0$, 88, 180°. At each of these three runs, frames were collected at 0.3° intervals and at 20 s per frame. At the end of these three runs, the first 100 frames were repeated in order to check that no alteration of the crystal had occurred during the experiment. The cell parameters were obtained from 504 reflections thresholded with a I/σ parameter of 20 at 298 K and 295 reflections with a I/σ parameter of 40. The diffraction frames were integrated using the SAINT package.[9] The structures were solved using the Siemens SHELXTL-plus package,[10] an absorption correction using the SADABS program[11] was applied.

The low spin state crystal structure determination of **1** was carried out using the Fddd diffractometer at Durham:[12] a four circle Huber goniometer, a Mo-Kα rotating anode (170 mA × 45 kV in this experiment) and a closed cycle cryorefrigerator. The quality of the crystal was first checked on the SMART CCD at room temperature. The sample was then enclosed in the Fddd beryllium cans, polaroid photographs were taken and cooling from room temperature to 11 K was performed at a rate of 0.3 K min^{-1}. At low temperature, polaroids which did not reveal new spots were taken. The cell parameters were obtained from the refinement of the positions of 25 reflections. The Bragg reflection intensity record consisted of ω scans of 96 steps, 1 s per step. Three reference reflections were monitored every 100 measured reflections showing no intensity deviation over the whole experiment. The structure was solved and refined using the above SHELXTL-package. A ψ-scan absorption correction, performed subsequently, showed no significant difference in the structures from corrected or non-corrected sets of data. The standard deviations on the atomic parameters are better in this case than in the two previous structures owing to a higher number of observed reflections.

In the three structures (298, 140 and 11 K), the hydrogen

atoms of the ligands are placed in geometrical positions. A molecule of methanol was found; it is statistically disordered and it was not possible to locate accurately the hydrogen atoms; we assume that they can only affect the intramolecular shape of the solvent. The complete formula of this compound is thus $Fe(PM\text{-}TeA)_2(NCS)_2 \cdot CH_3OH$.

The determination of the structural properties of **2** was performed using the Siemens SMART CCD as described above, both in the high (298 K) and low spin state (140 K), the same computing package being used. The cooling of the crystal was performed at a speed of 4 K min^{-1}. The crystal investigated was a black spearhead. The strategy of collection of the two sets of data was not exactly the same: the high temperature one was identical to the strategy described above for **1** although more frames were collected at low temperature for the last batches but a lower time per frame was used (10 s at 110 K *cf.* 20 s at 298 K). In both cases, the cell was determined from 512 reflections thresholded with a minimum I/σ of 50. The structural determination and refinement were performed with the above SHELXTL-plus package. The absorption correction made with SADABS slightly improved the refinement results.

Single crystals of **4** were black needles elongated along the *c*-axis. The quality of all the crystals used was first checked by rotating-crystal Weissenberg photographs. In general, they were of good quality and gave sharp and single Bragg reflections. The intensity data collections were performed using a Nonius CAD-4 diffractometer with graphite-monochromatized Mo-Kα ($\lambda = 0.71069$ Å) radiation. For low temperature measurements we used a cool dry nitrogen gas stream, the crystal being placed in a Lindemann tube and directly on the goniometer head of the diffractometer. The only way to ensure that the crystals undergo the transition without physical damage was not to irradiate them in the range 190–220 K. The cell parameter evolution was determined by cooling (9 sets of data) and warming (13 sets) at a rate of 1 K min^{-1} and with stopping points of *ca.* 2 h when searching the cell parameters. It is evident that, considering the large changes in the Bragg intensities occurring at the structural transition, the strategy of temperature variation affects strongly the parameter evolution curves. The cell parameters were determined using 25 selected reflections; this selection was different on both sides of the transition because of the dramatic changes in the Bragg reflection intensities that occurred. We checked the exact nature of the crystallographic change by following, as a function of temperature, the intensities of a set of reflections that has to become homologous with the transition from a monoclinic to an orthorhombic system. This test confirmed the very unusual aspect of this transition characterized by an increase of the symmetry as the temperature decreases. We also checked that no superstructure reflections appeared at low temperature. We collected two full sets of intensities for the structural determination at room temperature, 293 K, and in the low temperature state, at 140 K (Table 1). The intensities of three Bragg reflections were monitored every hour during data collection, and showed no deviations. A semi-empirical absorption ψ-scan correction was performed. The weakness of the ratio between the number of used reflections and the number of structural parameters arises from the low diffracting power of these crystals. The crystal structure of **4** (298 and 140 K) was solved with direct methods using the MITHRIL package[13] and the atomic coordinates were refined with locally written programs. The hydrogen atoms were placed in geometrical positions and only their atomic position coordinates were refined.[7]

The nature of the compound in the powdered form was checked by data collection on a Siemens powder diffractometer D500 equipped with a nitrogen cryosystem. This was done at 295 and 190 K after cooling, then at 295 K and at 330 K upon warming. The powder investigated had been used for several physical measurements.

Thermal analysis of the phase transition was performed on a Perkin-Elmer DSC apparatus using 11 mg of powder of **4**. Two thermal cycles were run cooling to 150 K and warming to 300 K with a speed of 2 K min^{-1} for the first complete cycle and 5 K min^{-1} for the second cycle. The weak energy exchanges lead to a very small signal and no reliable results could be extracted.

Full crystallographic details, excluding structure factors, have been deposited at the Cambridge Crystallographic Data Centre (CCDC). See Information for Authors, 1999, Issue 1. Any request to the CCDC for this material should quote the full literature citation and the reference number 1145/142.

3 Results

3.1 $Fe(PM\text{-}PEA)_2(NCS)_2$ 4

High spin state (298 K). This compound crystallises in the monoclinic system $P2_1/c$ and the asymmetric unit contains one molecule [Fig. 2(a)]. The atomic thermal vibrations are already small at room temperature. The Fe intramolecular environment is slightly unsymmetrical. The six Fe–N bond lengths and angles (Table 2) indicate a strong distortion, which appears to be common for a high spin state as well as the difference of *ca.* 0.15 Å between the $Fe\text{–}N_{cyan}$ and the $Fe\text{–}N_{pyr}$ bonds.[14–16] The Fe–NCS angles are 162 and 170° and the angle between the two NCS ligands is 96°. The network obtained by considering only the Fe atoms [Fig. 3(a)] is remarkable by the existence of relatively short distances between the iron atoms of adjacent molecules (i–$i_3 = 8.492$ Å).

The packing (Fig. 4) can be described as identical sheets of molecules in which each neighbouring molecule is in an antiparallel orientation, the NCS branches being separated by the ligand branches. A view of a layer is represented in Fig. 5(a). Intermolecular links are created through carbon–carbon and sulfur–carbon contacts. The molecular environment is not symmetrical; nevertheless, we have chosen to describe the topology of the interactions from the four nearest neighbours: the intrasheet interactions are characterized by the interatomic contacts between the original molecule i and the two neighbours i_1 and i_4 (Fig. 6) while the intersheet ones are defined by the two other molecules i_2 and i_3 as defined in Fig. 4 and 7. Table 3 lists distances between adjacent molecules shorter than the sum of the van der Waals distances as well as the corresponding iron–iron distances. The intersheet interactions are created by the arms of the NCS branches (Fig. 7) and correspond to the shortest Fe–Fe distances. The sulfur atoms create very close contacts with carbon atoms of the adjacent molecules in the intersheet direction, especially between S4 and carbon of the closer phenyl to the iron atom (S4···C25, S4···C24). One of the main characteristics of this structure is also the presence of strong intrasheet interactions created by very close contacts between carbon atoms of the phenyl cycles belonging to adjacent molecules. One of the shortest distances involves the triple bond [$C116\text{–}C35i_1 = 3.30(1)$ Å]. The length and number of these contacts mean that the molecules are linked to each other in a bidimensional network. Furthermore, taking into account the NCS–C intersheet contacts, a 3D system of intermolecular interactions could also be defined.

Low spin state (140 K). This compound undergoes a phase transition and, in the low spin state, belongs to the orthorhombic space group *Pccn*. The iron atom is located on a two-fold axis, which corresponds to an alignment of all the Fe atoms [Fig. 4(b)]. Thus, the Fe intramolecular environment becomes symmetrical. The Fe–N distances are significantly shortened (Table 2) and the N–Fe–N angles are closer to 90°, as generally observed for such transitions.[4,5,7,17,18] The Fe–N(PM-PEA) bonds in the LS form are shortened by 0.108 Å (Fe–N2),

Table 1 Crystal and experimental data for **1**, **2** and **4**

Compound	Fe(PM-PEA)$_2$(NCS)$_2$, **4**		Fe(PM-TeA)$_2$(NCS)$_2$, **1**			Fe(PM-AzA)$_2$(NCS)$_2$, **2**	
Formula	Fe $(C_{20}H_{13}N_2)_2(NCS)_2$		Fe $(C_{24}H_{18}N_2)_2(NCS)_2{\cdot}CH_3OH$			Fe $(C_{18}H_{13}N_4)_2(NCS)_2$	
Temperature/K	298	140	298	140	11	298	110
Spin state	HS	LS	HS	HS	LS	HS	LS
Crystal dimensions/mm	$0.75\times0.30\times0.15$	$0.50\times0.35\times0.20$	$0.80\times0.30\times0.20$	$0.80\times0.30\times0.20$	$0.44\times0.16\times0.16$	$0.50\times0.32\times0.20$	$0.50\times0.32\times0.20$
System	Monoclinic	Orthorhombic	Orthorhombic	Orthorhombic	Orthorhombic	Monoclinic	Monoclinic
Space group	$P2_1/c$	*Pccn*	*Pccn*	*Pccn*	*Pccn*	$P2_1/c$	$P2_1/c$
a/Å	15.637(1)	14.291(6)	17.048(1)	16.960(1)	16.759(7)	15.155(1)	15.038(1)
b/Å	14.566(8)	14.357(7)	15.098(1)	14.832(1)	14.611(7)	14.623(1)	14.396(1)
c/Å	16.821(1)	17.448(1)	16.983(1)	16.902(1)	16.852(7)	17.068(1)	16.677(1)
β/°	92.95(4)	90	90	90	90	92.95(1)	92.84(1)
V/Å^3	3826(4)	3580(4)	4371(1)	4252(1)	4135(4)	3777(1)	3605(1)
Refl. for cell (N)	25	25	504	295	25	512	512
Data collection	Nonius CAD-4	Nenius CAD-4	Siemens SMART-CCD	Siemens SMART-CCD	Huber-4	Siemens SMART CCD	Siemens SMART CCD
Radiation	MoKα	MoKα	MoKα	MoKα	MoKα	MoKα	MoKα
Scan type	ω	ω	ω	ω	ω	ω	ω
θ range/°	2–23	2–23	2–31	2–28	2–28	2–28	2–28
Measured	5446	5474	32839	28316	6297	27196	31321
Unique	4329	3397	6232	4861	4987	8639	8232
R_{int} (%)	1.8	2.0	10.4	6.6	1.6	5.2	4.9
h, min./max.	−17/17	−15/15	−24/24	−21/21	−16/21	−19/15	−19/19
k, min./max.	−1/17	−1/15	−19/21	−18/19	−19/1	−18/18	−18/18
l, min./max.	−1/17	−1/19	−24/23	−21/24	−1/22	−18/22	−21/21
μ/mm^{-1}	0.54	0.57	0.48	0.50	0.51	0.55	0.58
Absorption correction	ψ-scan	ψ-scan	SADABS	SADABS	ψ-scan	SADABS	SADABS
T, min./max.	0.926/1.00	0.926/1.00	0.396/0.838	0.629/0.828	0.964/0.976	0.675/0.828	0.818/0.914
Refinement against	F	F	F^2	F^2	F^2	F^2	F^2
Observed reflections $[I>2\sigma(I)]$	2318	1381	2454	3267	4325	4292	6226
Parameters (P)	460	230	277	277	277	460	460
R	0.054	0.040	0.061	0.049	0.049	0.063	0.043
$wR(F)/wR(F^2)$	0.054	0.041	0.131	0.097	0.115	0.168	0.105
S	1.1	1.0	1.1	1.0	1.0	1.0	1.0

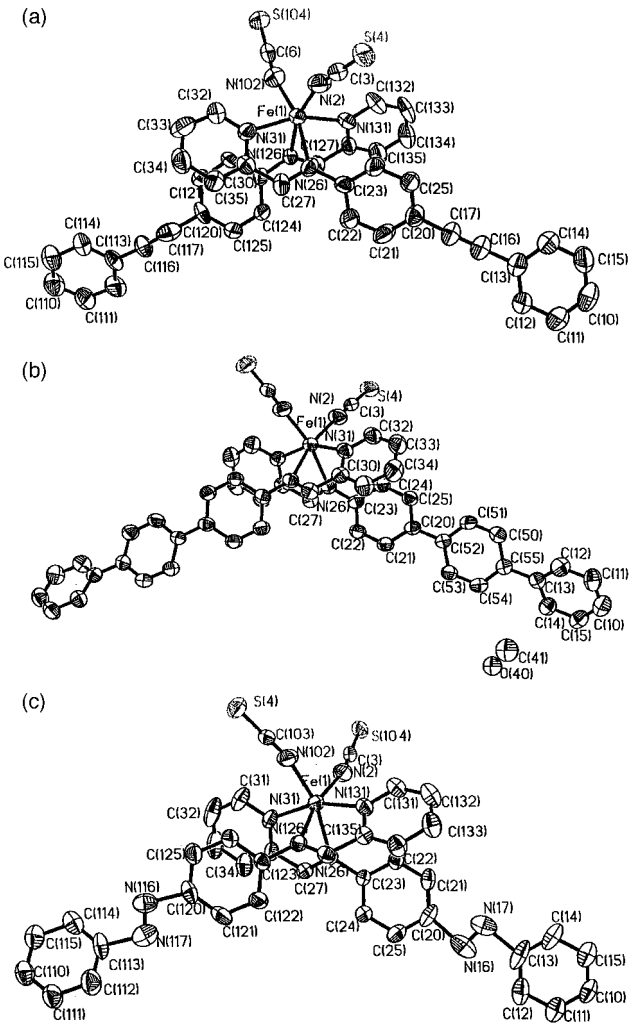

Fig. 2 Atom labeling for (a) **4**, (b) **1** and (c) **2**. Hydrogen atoms are omitted for clarity.

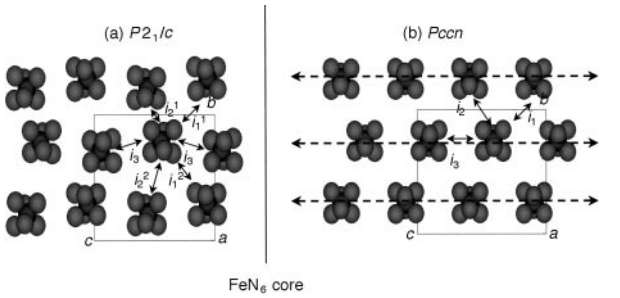

Fig. 3 Iron network (a) in $P2_1/c$ and (b) in *Pccn* structures. Only the FeN_6 cores are represented for clarity. The (a) type network is adopted in HS state by **4** and **2** and in the LS state by **2** only. The (b) type network is adopted by **4** in the LS state and by **3** and **1** in both HS and LS states. The nomenclature of the intermolecular interactions is also represented but the i_4 interaction which is perpendicular to the figure does not appear (see Fig. 6).

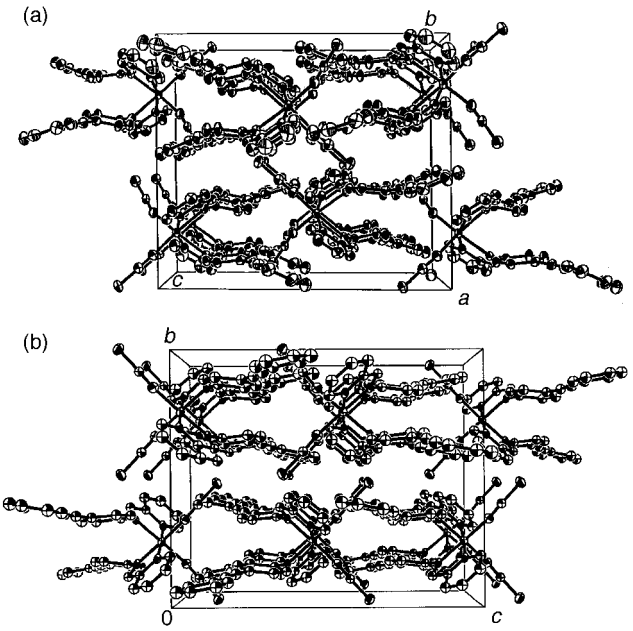

Fig. 4 View along *a* of the cell of **4** in (a) HS and (b) LS states.

0.216 Å (Fe–N31) and 0.275 Å (Fe–N26). Generally, the difference in Fe–N bond lengths between the HS and the LS states is in the range 0.16–0.21 Å.[19–21] The phenyl rings separated by the triple bond, in the low spin state, are inclined at an angle of 16.5° *cf.* 30 and 31° in the high spin state; this corresponds to a strong increase of the planarity of the ligands. The two NCS branches are strictly symmetrical; and form an angle of 90°. The Fe–NC(S) angle is 162°. The network created by the iron atoms has changed drastically in comparison with the high spin phase (Fig. 3). It is symmetrical in the low spin state with the iron atom lying on a special position. The nearest iron atoms are significantly closer in the high spin network (by 0.24 Å, Table 3). This evolution is not systematic but has already been encountered in previous spin crossover structural studies. The shape of the NCS arms significantly changes (Fig. 6 and 8), resulting in intersheet sulfur–carbon contacts slightly longer in the low spin phase (Table 3). The carbon–carbon intrasheet contacts also appear to be longer in the low spin phase. These changes correspond to a symmetrization of the whole molecular environment. Moreover, the

Table 2 Iron intramolecular environment, distances (Å) and angles (°). Standard deviations are less than 0.003 Å and 0.1°

	$Fe(PM\text{-}PEA)_2(NCS)_2$		$Fe(PM\text{-}TeA)_2(NCS)_2$			$Fe(PM\text{-}AzA)_2(NCS)_2$		$Fe(PM\text{-}BiA)_2(NCS)_2$[a]	
	298 K	140 K	298 K	140 K	11 K	298 K	110 K	298 K	140 K
Fe–N2	2.056	1.948	2.082	2.051	1.972	2.060	1.948	2.041	1.939
Fe–N102	2.055	1.948	2.082	2.051	1.972	2.059	1.944	2.041	1.939
Fe–N31	2.164	1.946	2.181	2.126	2.037	2.172	1.978	2.230	1.964
Fe–N131	2.167	1.946	2.181	2.126	2.037	2.157	1.967	2.230	1.964
Fe–N26	2.246	1.971	2.259	2.184	2.054	2.270	1.989	2.251	1.966
Fe–N126	2.270	1.971	2.259	2.184	2.054	2.246	1.979	2.251	1.966
N2–Fe–N102	96.0	90.2	95.2	93.5	91.58	95.7	90.5	93.4	88.0
N2–Fe–N26	93.1 (94.5)	92.7	93.8	93.9	93.08	94.6 (92.6)	93.2 (91.2)	96.0	93.1
N2–Fe–N31	101 (99.4)	95.2	93.0	92.5	92.78	98.6 (100.4)	90.6 (92.5)	90.2	90.8
N31–Fe–N26	73.8 (74.2)	79.7	74.1	75.9	78.75	73.9 (74.4)	80.6 (80.4)	74.3	80.7

[a]From ref. 5 and 7.

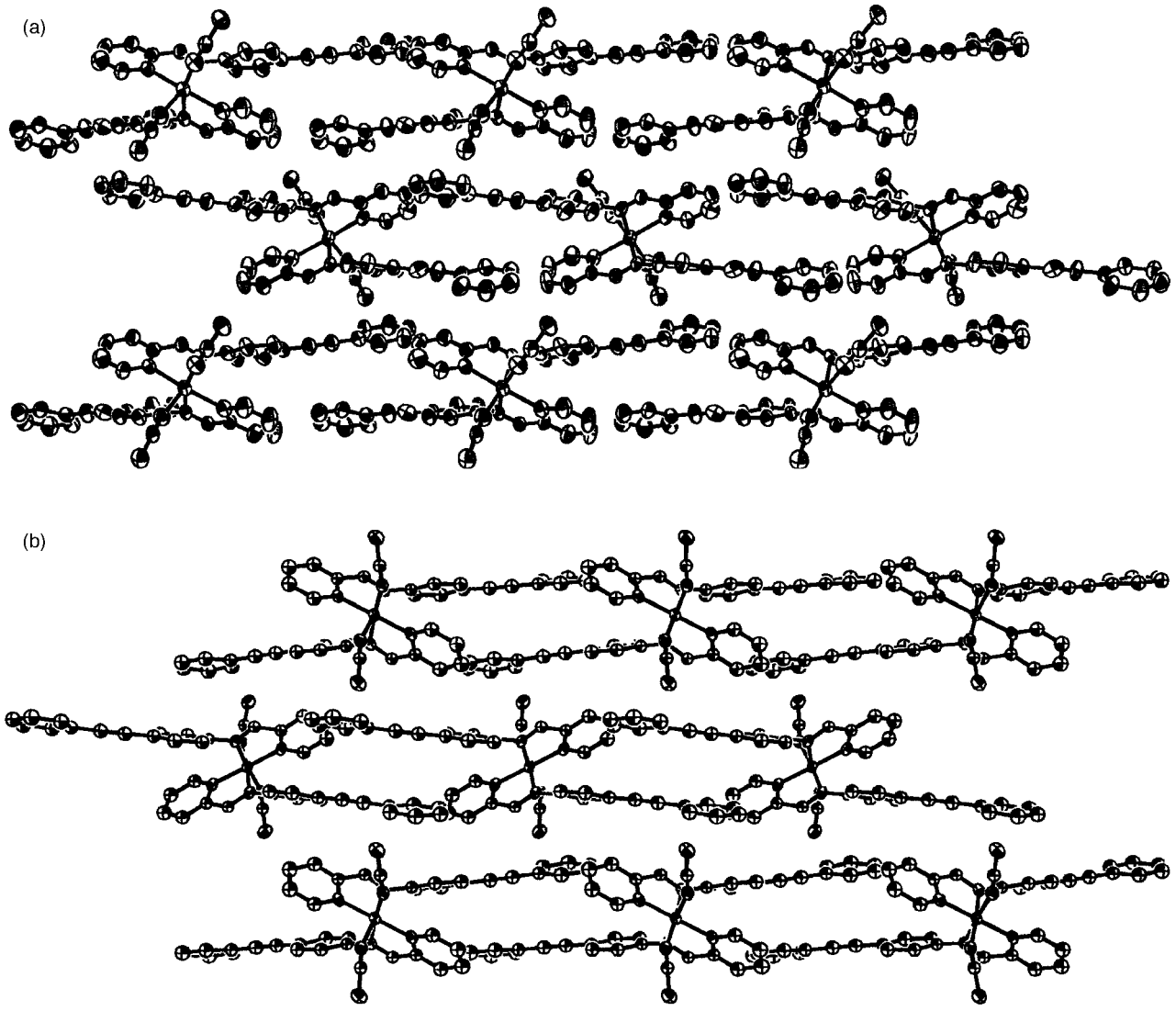

Fig. 5 View along *c* of a layer in **4** in (a) in HS and (b) LS states.

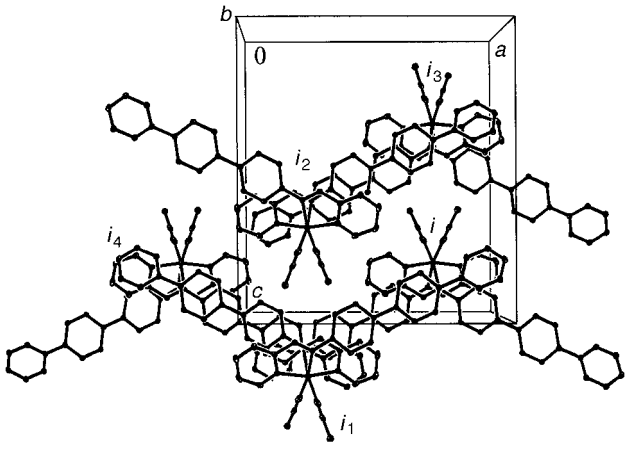

Fig. 6 Schematic view and nomenclature of the four described intermolecular interactions (shown for **1**). i–i_1 and i–i_4 correspond to intrasheet interactions and i–i_3 and i–i_2 to intersheet ones.

angles between the phenyl rings of adjacent molecules are very different in the two structures: in the high spin state the four angles involved in the shortest interactions are 40.5, 40.3, 25.0 and 14° whilst in the low spin state they decrease to 19.1, 7.7, 19.4 and 4.0°, respectively. Thus, it is clear that the topology of the network interactions is quite different in the high and low spin state structures.

Thermal contraction (298 to 110 K). The cell parameters of this compound evolve continuously and slightly on both sides of the transition in the range 298–220 K and 180–110 K. The relative dependence of the cell parameters and the volume (Fig. 8) shows the sharpness of the transition that occurs in the range 210 to 190 K. Within this interval, the *c* parameter increases by *ca.* 4% (corresponding to the interaction i–i_4), the *b* parameter decreases by *ca.* 9% (interaction i–i_1), the *a* parameter remains almost constant (intersheet) and β decreases by 3°. Thus, the anisotropic character of the cell parameters changes at the transition point is strong. The volume decreases by 240 Å^3 (6.4%) in the range 293–130 K. The volume variation *vs.* temperature corresponds to the sum of two effects: the thermal contraction, ΔV_T, and the contraction due to the spin crossover transition, ΔV_{SC}. These two contributions can be estimated from Fig. 8, in the range 293–130 K, $\Delta V_T \approx 150$ Å^3 and $\Delta V_{SC} \approx 90$ Å^3, corresponding, respectively, to 4.0 and 2.4% of the volume at room temperature. The estimated contraction due to the spin crossover transition is very close to that obtained in the low temperature and high pressure studies of the two spin crossover compounds $Fe(phen)_2(NCS)_2$ (phen = 1,10-phenanthroline) and $Fe(btz)_2(NCS)_2$ (btz = 2,2′-bis(4,5-dihydrothiazine)).[17,18,22,23]

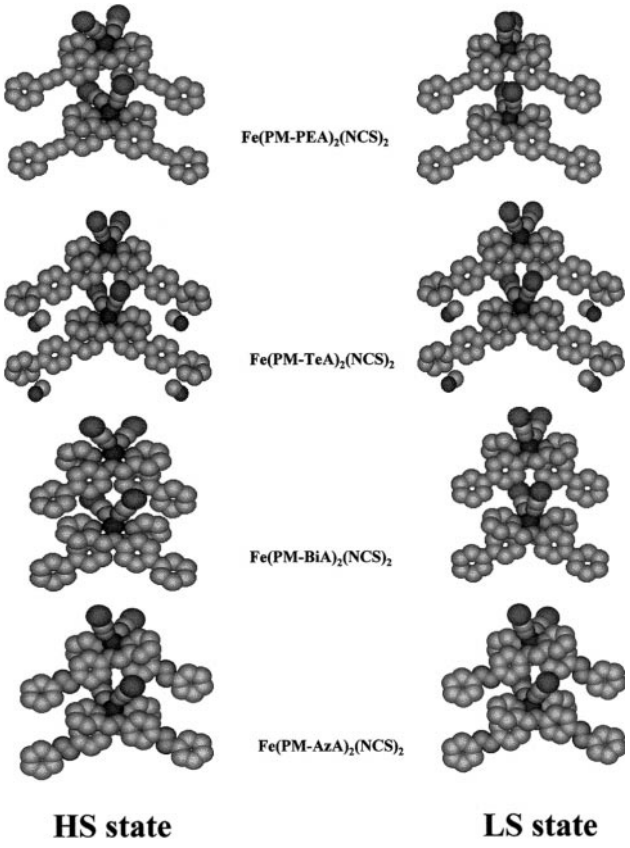

Fig. 7 View of the intersheet interaction i–i_3 for the four Fe(PM-L)$_2$(NCS)$_2$ compounds in HS and LS states.

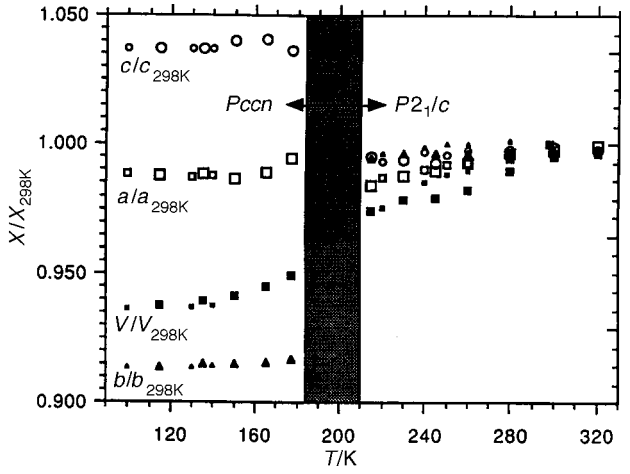

Fig. 8 Relative cell parameters and temperature dependence of the cell volume of **4**.

The results are not accurate enough to confirm or otherwise the presence of a large structural hysteresis; the lack of supplementary values is due to the fragility towards irradiation of the crystals in the range 190–220 K.

The powder diffraction analyses show that the powder phase is identical to the single crystal in both LS and HS states; in Fe(PM-BiA)$_2$(NCS)$_2$ the existence of different phases at room temperature was proved from powder measurements,[6] which emphasized that physical and crystallographic measurements should be performed on the same sample.

3.2 Fe(PM-TeA)$_2$(NCS)$_2$ 1

HS state (298 K and 140 K). This compound crystallises in the orthorhombic space group, *Pccn*, and the asymmetric unit contains one half molecule [Fig. 2(b)] which lies on a two-fold axis, the iron atom being in a special position. Therefore, the intramolecular environment of the iron is symmetric; the angles and distances correspond to a high spin state both at 298 and 140 K. Nevertheless, the significant decrease of the iron–nitrogen bond lengths is consistent with the beginning of a transition towards a low spin state. The Fe–NCS angle is 170° at 298 K and 171° at 140 K.

To a first approximation the packing of the molecules for **1** is similar to that for **4** in the LS state. The molecules define sheets where the neighbours are linked to each other through short carbon–carbon contacts. This packing can be defined by the same four kinds of interactions used previously, two intrasheet ones (i–i_1 and i–i_4) and two intersheet ones (i_2 and i_3) (Fig. 7 and 8, Table 3). The iron–iron distance corresponding to the i_3 interaction is very short and creates S–C contacts, slightly shorter at 140 K. Such contacts exist also in the intersheet i_2 interaction but in both no carbon–carbon contacts are observed. The iron–iron distance corresponding to i_4 is long and no contacts exist between the two molecules. This can be related to the presence of a molecule of methanol that does not allow the two ligands of the two molecules to be close in that direction. Many C–C contacts link the i and i_1 intrasheet molecules and very short ones (3.34 Å) exist at low temperature. However, the structures at 298 and 140 K are very similar and the global evolution of the packing corresponds only to the thermal contraction.

LS state (11 K). As expected from the magnetic properties, no large structural phase transition occurs; the cooling of the sample simply induces a contraction of the cell. The intramolecular angles between the three phenyl groups are quite high at room temperature and do not change significantly on cooling: 31.5° at 298 K, 29.9° at 140 K and 27.7° at 11 K between the C20 ring and the C10 ring and 25.3, 25.6 and 26.3° between the C20 ring and the C50 ring. Thus, the planarity increases very slightly when cooling. The Fe–N bond lengths and the values of the corresponding angles, closer to 90°, (Table 2) are consistent with the occurrence of the spin crossover transition. Nevertheless, the Fe–N31 and Fe–N26 bond contractions [0.144(2) and 0.205(2) Å, respectively] are less pronounced than the previous one for the same family (*i.e.* compound **4**), suggesting that the spin conversion is not complete, even at 11 K. The iron atom network remains essentially identical with slight decreases of the Fe–Fe distances induced by the cell contraction. Even at 11 K no very short C–C intersheet contacts exist. The intrasheet contacts decrease, leading to very short interactions in the i–i_1 direction. This decrease appears almost continuous from 298 to 11 K. No short contact is created between the i and i_4 molecules. The crystal structure variations of **1** from 298 to 11 K are weak and continuous, in agreement with the magnetic behaviour.

At 298 K, the carbon atom of the solvent molecule, which is near a two-fold axis, is statistically disordered while it lies on the two-fold axis at low temperature. Moreover, the thermal displacement parameters of this atom decrease by a factor of three from 298 K [$U_{eq} = 184(8) \times 10^{-3}$ Å^2] to 140 K [$63(7) \times 10^{-3}$ Å^2] while those of the other carbon atoms of the main molecules only decrease by a factor of two. The decrease of this parameter is almost identical for all other carbon atoms from 140 to 10 K. Thus, the solvent molecule undergoes an ordering from 298 to 140 K. This is consistent with the study of [Fe(α-pic)$_3$]Cl$_2$·EtOH (α-pic = α-picoline = 2-methylpyridine) where a similar ordering has been considered as the initiator of the spin transition.[24]

3.3 Fe(PM-AzA)$_2$(NCS)$_2$ 2

HS state (298 K). this compound crystallizes in the monoclinic space group $P2_1/c$ and the asymmetric unit contains one molecule [Fig. 2(c)]. The iron environment is slightly unsym-

metrical. The phenyl rings are not coplanar and form angles of 28.5° (C10 group and C20 group) and 32.5° (C110 and C120). At first glance, the crystal structure appears to be very similar to that adopted by **4** at high temperature and can be described with the same interactions i, i_1, i_2, i_3 and i_4. Nevertheless, only a few weak intersheet interactions are found through sulfur–carbon contacts and no short C–C contacts are observed (Table 3). A small number of strong intrasheet interactions exist, the strongest involving the nitrogen atom of the azo group (N117–C27 $i_1 = 3.494$ Å). The interaction between the two farthest neighbours i and i_4 is significant and this also involves the nitrogen of the azo group (N17–C14 $i_4 = 3.544$ Å).

LS state (110 K). No phase transition occurs and the cell parameters simply decrease as a result of thermal effects. The volume is reduced by 172 Å^3 from 298 to 110 K. The Fe–N distances correspond to those expected for a low spin state; the shortening of Fe–N26 [0.281(2) Å] and Fe–N126 [0.267(2) Å] from the high to the low spin state is very large. The FeN_6 core is slightly more symmetrical due to the N–Fe–N angles that are all close to 90°. The intramolecular phenyl rings are still non-coplanar and the angles between them change slightly to 25.6 and 35.3°, respectively. The intramolecular angles in the azo group strongly increase from 298 K to 110 K: from 94.5 to 113.8° (C13, N17, N16), from 92.3 to 112.1 (C20, N16, N17), from 103.3 to 112.9° (C110, N117, N116) and from 103.3 to 114.5° (C120, N116, N117). So, from this point of view, the molecule appears to be more symmetrical in the low spin state. The intersheet interactions are similar to those at high temperature, with no short ones being found. The intrasheet distances decrease leading to a very short i–i_4 interaction (N17–C14 $i_4 = 3.346$ Å).

4 Discussion

4.1 Thermal contraction

Compounds **1**, **3** and **4** adopt the same crystallographic space group, *Pccn*, at low temperature, **1** and **3** crystallize also in this space group at room temperature while **2** and **4** crystallize in the monoclinic $P2_1/c$ space group in the HS state. The volume reduction per degree of temperature from the HS to the LS state is largest (1.5 Å^3 K^{-1}) for **4**, which is the only one to undergo a phase transition while the values are similar for **3** (0.78 Å^3 K^{-1}), **1** (0.82 Å^3 K^{-1}) and **2** (0.91 Å^3 K^{-1}) as well as in previously reported similar compounds $Fe(phen)_2(NCS)_2$ and $Fe(btz)_2(NCS)_2$ (0.74 and 0.76 Å^3 K^{-1}, respectively). The reduction of the volume corresponding to the spin transition itself has been estimated from the temperature dependence curves to be 2.4% for **4** and 1.9% for **3**. In order to estimate this reduction for **1**, we could, in a first approach, compare its volume variation to those of some molecular charge transfer compounds, which do not undergo spin crossover but which have been studied systematically in this range of temperature (298–10 K) and which have similar unit cell volume.[25] As a common trend, they showed a volume contraction from 298 to 10 K of 3–4%. The unit cell volume of **1** decreases by 5.4% from 298 to 10 K, which suggests a volume contraction due to the spin transition to be in the range 1.5–2.5%. This estimated value is consistent with previous values and could be a general trend for these compounds. Indeed, $Fe(phen)_2(NCS)_2$ and $Fe(btz)_2(NCS)_2$ presented very similar values, 2.5 and 2.2%, respectively.

It is worth remarking that the spin transition upon cooling is accompanied by a strong increase of the c parameter (intersheet directions) only for **3** and **4** which are the only compounds of the series that present an abrupt transition.

4.2 Iron atom network and iron environment

Iron atom network. The main difference between these spin transitions is that a large structural phase transition occurs only in **4** with a change in space group and in the relative positions of the centers of gravity of the molecules. In this compound and in **2**, the iron atom is not in a special position at room temperature and so the iron network appears to be less symmetrical than in the two other compounds (Fig. 2). At low temperature, the phase transition in **4** results in a more

Table 3 List of the shortest intermolecular distances (Å) for $Fe(PM\text{-}L)_2(NCS)_2$ with the corresponding Fe–Fe distances[a]

	$Fe(PM\text{-}PEA)_2(NCS)_2$		$Fe(PM\text{-}BiA)_2(NCS)_2$		$Fe(PM\text{-}TeA)_2(NCS)_2$			$Fe(PM\text{-}AzA)_2(NCS)_2$	
	298 K	140 K	298 K	140 K	298 K	140 K	11 K	298 K	110 K
Fe–Fe i_1^1/i_1^2	11.710/13.868	12.327	11.708	11.269	13.206	13.031	12.779	11.529/13.501	11.144/13.081
Fe–Fe i_2^1/i_2^2	11.109/9.037	10.293	10.331	10.176	11.528	11.425	11.330	9.115/10.914	9.197/10.888
Fe–Fe i_3	8.491	8.734	8.805	9.141	8.491	8.451	8.426	8.603	8.396
Fe–Fe i_4	15.637	14.291	12.949	12.370	17.048	16.960	16.759	15.155	15.037
i–i_2 S–C	3.65	3.767	3.416	3.437	3.600	3.579	3.619	3.721	3.734
S–C	3.46	3.588	3.608	3.764					
i–i_3 C–C	3.62								
C–C			3.457	3.409					
C–S	3.74	3.551	3.776	3.818	3.673	3.626	3.601	3.753	3.691
i–i_1 C–S	—	—	3.348	3.416	—	—	—	3.746	3.646
C–C	3.56	3.503	3.406	3.602	3.513	3.473	3.426	3.687	3.606
	3.62	3.647	3.464	3.500	3.608	3.605	3.518	3.646	3.646
	3.64	3.449	3.684	3.522	3.593	3.556	3.535	3.667	3.552
	3.57	3.629	3.599	3.456	3.567	3.556	3.553		
	3.54	3.492	3.683	3.571	3.564	3.545	3.521	C–N(AzA)	C–N(AzA)
	3.62	3.476	3.599	3.456	3.393	3.338	3.295	3.494	3.422
	3.60				3.533	3.521	3.494	3.634	3.583
	3.30				3.556	3.491	3.478		
	3.62				3.647	3.579	3.551		
	3.51								
	3.40							i–i_4 C–N(AzA)	
	3.61							3.615	3.493
	3.55							3.544	3.346
i–i_4 C–C	3.50	3.476	3.657	3.337				3.660	3.466

[a]Contacts are considered short for C–C <3.65 Å and S–C 3.75 Å. Standard deviations are <0.02 Å in $Fe(PM\text{-}PEA)_2(NCS)_2$ (298 K) and 0.01 Å in the others. The nomenclature i, i_1, i_2, i_3 and i_4 is defined in Fig. 3 and 6. i–i_1 and i–i_4 correspond to intrasheet interactions while i–i_2 and i–i_3 correspond to intersheet ones.

symmetrical network which becomes, in that sense, similar to those of **1** and **3**. In all the structures, the shortest Fe–Fe distance is observed between the two neighbouring molecules in the *c* direction (Table 3, interaction i–i_3). As a consequence of the increase of this parameter when cooling, the shortest Fe–Fe distance is longer at low temperature in Fe(PM-PEA)$_2$(NCS)$_2$ and Fe(PM-BiA)$_2$(NCS)$_2$, than in Fe(PM-TeA)$_2$(NCS)$_2$ or Fe(PM-AzA)$_2$(NCS)$_2$.

Iron environment. The changes in the FeN_6 core are quite similar in all the complexes upon changing from high to low spin (Table 2). All the N–Fe–N angles converge to 90° upon transformation to the LS state. The contraction of the Fe–N bond lengths appears to be similar in **2**, **3** and **4** (the spin conversion is not complete for **1**): the normalized values of the variation of these distances between HS and LS show a similar evolution of the Fe–N2 bond (*ca.* 5%) for all the compounds, whilst this is not the case for Fe–N31 (11.9% for **3**, 10.1% for **4**, 6.6% for **1** and 8.9% for **2**) or for Fe–N26 (12.7, 12.8, 9.1 and 12.1%, respectively). The Fe–N31 changes were 8.5% for Fe(btz)$_2$(NCS)$_2$ and 8.4% for Fe(phen)$_2$(NCS)$_2$ and 9.4% for Fe–N26. These values reflect the large variations which occur in the Fe–N26 and Fe–N31 bond lengths **1–4** at the transition. Indeed, the corresponding Fe–N26 and Fe–N31 bond length changes in Fe^{II} compounds have always been reported[26] to be within the range 0.15–0.20 Å while the variation, in the present study, reaches 0.299 Å in **4**, 0.285 Å in **3** and 0.281 Å in **2**. This remarkable evolution arises from unusually long Fe–N26 and Fe–N31 bond lengths in the HS state together with usual values in the LS state. We can also see that these shift values are close to the Fe–P values (0.28 Å) in Fe(dppen)$_2$Cl$_2$·2(CH$_3$)$_2$CO [dppen = *cis*-1,2-bis(diphenylphosphino)ethylene].[27] The same observation has been made for compounds with the $Fe^{II}P_4X_2$ core, where Fe–P bond lengths vary by as much as 0.27 Å between the LS and HS state.[28] For Fe(PM-BiA)$_2$(NCS)$_2$ at 10 K, a LIESST (light induced excited spin state trapping) effect has been observed.[5] The HS→LS relaxation after LIESST was investigated between 10 and 78 K and revealed a very slow rate of quantum mechanical tunneling. Such an effect has been attributed to the unusually large change in Fe–N (organic ligand) bond lengths associated with the spin transition.

4.3 Intersheet and intrasheet interactions

Intersheet interactions. Although **3** also develops short C–C contacts, the intersheet interactions involve mainly sulfur–carbon contacts (Table 3). These contacts are short for **4** and **3**, slightly longer for **1** and the longest are generated in **2**. The NCS branches form arms that clasp neighbouring molecules in the *c* direction. A significant change in the shape of the NCS arms occurs during the spin conversion for **3** and **4** but not for **1** and **2**, as shown in Fig. 7.

Intrasheet interactions. In the high spin state, the shortest intrasheet contacts are observed in **4**. Nevertheless, considering the i–i_1 molecules, the intrasheet interaction appears, in a first approach, to be similar in the four compounds, with numerous short C–C contacts being formed. However, from the number of very short distances (<3.5 Å), the interactions created in **3** appear to be the strongest and those of **2** the weakest. The variation upon cooling appears to be different: for instance, the shortest distances from 298 to 140 K increase in **4** (3.30 to 3.45 Å) and **3** (3.348 to 3.416 Å) but decrease in **2** (C–N: 3.494 to 3.422 Å) and in **1** from 298 to 11 K (3.393, 3.338 and 3.295 Å). One of the main differences between Fe(PM-TeA)$_2$(NCS)$_2$ and the three other compounds is the absence of short phenyl C–C contacts belonging to the molecule *i* and the molecule $i+a$, denoted i_4. Such interactions between 'second neighbours' are strong in **3** and **4** at room temperature, emphasizing the strength of the intermolecular links in these two structures. The increase of the length of the [PM-L] ligands from Fe(PM-BiA)$_2$(NCS)$_2$ to Fe(PM-TeA)$_2$(NCS)$_2$ results in an increase of the cell parameter *a* which corresponds to the i–i_4 interaction. However, without the presence of solvent which hinders this 'second neighbour' interaction, the overlap of *i* and i_4 could be strong. Thus, even if the greater length of the ligands in Fe(PM-TeA)$_2$(NCS)$_2$ probably strongly favours inclusion of solvent, it would be very interesting to obtain the non-solvated compound. Further work along this line is in progress.

4.4 Abruptness of the transition

Some papers have concluded that the abruptness of the transition in this kind of iron(II) complex[17] could be understood from the intrasheet interactions; this conclusion was reached by comparing the structures of only one iron complex with an abrupt transition to another with a quite smooth transition, the intrasheet interactions being much stronger in the former. Nevertheless, the intersheet contacts were strong in both complexes. In the present series, we cannot assign the abruptness of the transition to only the strength of the intrasheet interactions as they are quite strong in **1** and **2**, which undergo smooth transitions. On the other hand, the intersheet interactions are weaker in **1** and **2** than in the two other compounds. The latter also develops poor contacts between intrasheet second neighbour molecules. Thus, if strong intrasheet interactions are obviously required to obtain an abrupt transition, it is the whole topology of the interaction which has to be taken into account to explain the differences in the abruptness of the transitions. The softness of the transition in **1** is attributed to the presence of the solvent which prevents intersheet and long range intrasheet contacts. Taking into account all the interactions, **3** adopts the most compact structure of the four complexes, even if the shortest C–C distance is found in **4** which has a more irregular packing. The relative softness of the transition for **2** is clearly related to the global topology of interactions that is less favorable than for **3** or **4**. At this point, we can note that the shortest intermolecular distances in Fe(PM-PEA)$_2$(NCS)$_2$ and in Fe(PM-AzA)$_2$(NCS)$_2$ involve the –C≡C– bond and the –N=N– bond, respectively. The only chemical difference between the two complexes resides in the –C≡C– *vs.* –N=N– bonds. This difference induces dramatic effects as far as the spin transition is concerned.

4.5 Hysteresis width

There is a significant hysteresis effect only in **4** which is also the only compound that undergoes a crystallographically significant structural phase transition. The low and high temperature structures are quite different as the former presents an iron atom network and a topology of interactions which is much more symmetrical. The hysteresis effect is then obviously due to the differences in the HS and LS structures in this complex. Such a phase transition cannot occur in **1** or **3** because these compounds already adopt symmetrical networks, with the iron atoms on a two fold axis at room temperature in the HS state. The iron network in **2** appears similar to that in **4** although no phase transition occurs. This difference can be connected to the weakest interaction topology in **2** and to the shortest interaction found in **4**. The strength and the asymmetry of the interactions in **4** could lead to a necessary rearrangement of the global network at the spin conversion while the highest flexibility of the packing in **2** could support both the thermal contraction and the spin conversion without reorganisation. Thus, in the case of Fe(PM-PEA)$_2$(NCS)$_2$ which presents an unusually large hysteresis, it is the large structural phase transition which governs the spin conversion features.

The magnetic behaviour of these complexes under high pressure has been investigated;[6] the pressure strongly affects the temperature of transition as well as the hysteresis width. A high pressure X-ray diffraction study is in progress in our laboratories.

Acknowledgements

P.G. thanks the European Community for the benefit of the Marie Curie TMR European grant ERB4001GT964249. J.A.K.H. thanks the University of Durham for a Sir Derman Christopherson Foundation Fellowship. We are grateful for financial support from the European Commission for granting the TMR-Network 'Thermal and Optical Switching of Spin States (TOSS)', Contract No. ERB-FMRX-CT98–0199.

References

1 H. A. Goodwin, *Coord. Chem. Rev.*, 1976, **18**, 293; P. Gütlich, *Struct. Bonding (Berlin)*, 1981, **44**, 83; E. König, *Prog. Inorg. Chem.*, 1987, **35**, 527; P. Gütlich and A. Hauser, *Coord. Chem. Rev.*, 1990, **97**, 1; P. Gütlich, A. Hauser and H. Spiering, *Angew. Chem., Int. Ed. Engl.*, 1994, **33**, 2024 and references therein; P. Gütlich, J. Jung and H. A. Goodwin, *Molecular magnetism: from Molecular Assemblies to the devices*, NATO ASI Ser. E, ed. E. Coronado, 1996, vol. 321, pp. 327–378.

2 O. Kahn and J. P. Launay, *Chemtronics*, 1988, **3**, 140; J. Zarembovitch and O. Kahn, *New. J. Chem.*, 1991, **15**, 181; O. Kahn, *Molecular Magnetism*, VCH, New York, 1993.

3 W. Vreugdenhil, J. H. van Diemen, R. A. G. de Graaf, J. G. Haasnoot, J. Reedgijk, A. M. Kraan, O. Kahn and J. Zarembovitch, *Polyhedron*, 1990, **9**, 2971; O. Kahn, J. Kröber and C. Jay, *Adv. Mater.*, 1992, **4**, 178; J. Krôber, J. P. Audière, R. Claude, E. Codjovi, O. Kahn, J. G. Haasnoot, F. Grolière, C. Jay, A. Bousseksou, J. Linarès, F. Varret and A. Gonthier-Vassal, *Chem. Mater.*, 1994, **6**, 1404; L. G. Lavrenova, V. N. Ikorskii, V. A. Varnek, I. M. Oglezneva and S. V. Larionov, *Polyhedron*, 1995, **14**, 1333; G. Lemercier, M. Verelst, A. Bousseksou, F. Varret and J. P. Tuchagues, *Magnetism: A Supramolecular Function*, NATO ASI Ser. E, ed. O. Kahn, Kluwer Academic, 1996, pp. 335–356.

4 J. F. Létard, P. Guionneau, E. Codjovi, L. Olivier, G. Bravic, D. Chasseau and O. Kahn, *J. Am. Chem. Soc.*, 1997, **199**, 10861.

5 J. F. Létard, P. Guionneau, L. Rabardel, J. A. K. Howard, A. E. Goeta, D. Chasseau and O. Kahn, *Inorg. Chem*, 1998, **37**, 4432. We recall the cell parameters values in HS state (298 K): orthorhombic, *Pccn*, $a=12.949(7)$, $b=15.183(2)$, $c=17.609(5)$ Å, $V=3462(2)$ Å^3, $R=0.045$ and in LS state (140 K): orthorhombic, *Pccn*, $a=12.370(3)$, $b=14.764(3)$, $c=18.281(4)$ Å, $V=3338(2)$ Å^3, $R=0.043$.

6 V. Ksenofontov, G. Levchenko, H. Spiering, P. Gütlich, J. F. Létard, Y. Bouhedja and O. Kahn, *Chem. Phys. Lett.*, 1998, **294**, 545.

7 J. F. Létard, S. Montant, P. Guionneau, P. Martin, A. Le Calvez, E. Freysz, D. Chasseau, R. Lapouyade and O. Kahn, *Chem. Commun.*, 1997, 745. See the journal instructions to obtain the corresponding. cif files.

8 SMART Version 4.050, Siemens Analytical X-ray Instruments, Madison, WI, 1995.

9 SAINT Version 4.050, Siemens Analytical X-ray Instruments, Madison, WI, 1995.

10 G. M. Sheldrick, SHELXTL-Plus, Release 4.1, Siemens Analytical X-ray Instruments Inc., Madison, WI, 1991.

11 G. M. Sheldrick, SADABS Empirical Absorption Program, Univ. of Gottingen, 1995.

12 R. C. B. Copley, A. E. Goeta, C. W. Lehmann, J. Cole, D. S. Yufit, J. A. K. Howard and J. Archer, *J. Appl. Crystallogr.*, 1997, **30**, 413.

13 C. J. Gilmore, MITHRIL, *J. Appl. Crystallogr.*, *Sect. B*, 1984, **17**, 42.

14 C. Roux, J. Zarembovitch, B. Gallois, T. Granier and R. Claude, *Inorg. Chem.* 1994, **33**, 2273.

15 E. König and K. J. Watson, *Chem. Phys. Lett.*, 1970, **6**, 457.

16 G. Vos, R. A. G. de Graaf, J. G. Haasnot, A. M. van der Kraan, P. de Vaal and J. Reedijk, *Inorg. Chem.*, 1984, **23**, 2905.

17 J. A. Real, B. Gallois, T. Granier, F. Suez-Panama and J. Zarembovitch, *Inorg. Chem.*, 1992, **31**, 4972.

18 B. Gallois, J. A. Real, C. Hauw and J. Zarembovitch, *Inorg. Chem.*, 1990, **29**, 1152.

19 M. A. Hoselton, L. J. Wilson and R. S. Drago, *J. Am. Chem. Soc.*, 1975, **97**, 1722.

20 M. Mikami and Y. Saito, *Acta Crystallogr.*, *Sect. B*, 1982, **38**, 452.

21 L. Wiehl, G. Kiel, C. P. Köhler, H. Spiering and P. Gütlich, *Inorg. Chem.*, 1986, **25**, 1565.

22 J. Gaultier, T. Granier, B. Gallois, J. A. Real and J. Zarembovitch, *High Pressure Res.*, 1991, **7**, 336.

23 T. Granier, B. Gallois, J. Gaultier, J. A. Real and J. Zarembovitch, *Inorg. Chem.*, 1993, **32**, 5305.

24 M. Mikami, M. Konno and Y. Saito, *Acta Crystallogr.*, *Sect. B*, 1980, **36**, 275.

25 P. Guionneau, J. Gaultier, D. Chasseau, G. Bravic, Y. Barrans, L. Ducasse, D. Kanazawa, P. Day and M. Kurmoo, *J. Phys. I Fr.*, 1996, **6**, 1581; P. Guionneau, C. J. Kepert, M. Rosseinsky, D. Chasseau, J. Gaultier, M. Kurmoo, M. B. Hursthouse and P. Day, *J. Mater. Chem.*, 1997, **7**, 367; D. Chasseau, J. Gaultier, G. Bravic, L. Ducasse, M. Kurmoo and P. Day, *Proc. R. Soc. London Ser. A*, 1993, **442**, 207.

26 J. K. McCuster, A. L. Rheingold and D.N. Hendrickson, *Inorg. Chem.*, 1996, **35**, 2100; E. König, *Struct. Bonding* (*Berlin*), 1991, **76**, 51.

27 F. Cecconi, M. DiVaira, S. Midollini, A. Orlandini and L. Sacconi, *Inorg. Chem.*, 1981, **20**, 2043.

28 C.-C. Wu, J. Jung, P. K. Gantzel, P. Gütlich and D. N. Hendrickson, *Inorg. Chem.*, 1997, **36**, 5339.

Paper 8/08075E